The Astrophysical Journal, 824:37 (7pp), 2016 June 10 doi:10.3847/0004-637X/824/1/37

NUSTAR AND *XMM-NEWTON* OBSERVATIONS OF THE NEUTRON STAR X-RAY BINARY 1RXS J180408.9-34205

R. M. Ludlam[1], J. M. Miller[1], E. M. Cackett[2], A. C. Fabian[3], M. Bachetti[4], M. L. Parker[3], J. A. Tomsick[5], D. Barret[6,7], L. Natalucci[8], V. Rana[9], and F. A. Harrison[9]

[1] Department of Astronomy, University of Michigan, 1085 South University Ave., Ann Arbor, MI 48109-1107, USA
[2] Department of Physics & Astronomy, Wayne State University, 666 W. Hancock St., Detroit, MI 48201, USA
[3] Institute of Astronomy, Madingley Road, Cambridge CB3 0HA, UK
[4] INAF/Osservatorio Astronomico di Cagliari, via della Scienza 5, I-09047 Selargius (CA), Italy
[5] Space Sciences Laboratory, 7 Gauss Way, University of California, Berkeley, CA 94720-7450, USA
[6] Universit de Toulouse; UPS-OMP; IRAP; Toulouse, France
[7] CNRS; Institut de Recherche en Astrophysique et Plantologie; 9 Av. colonel Roche, BP 44346, F-31028 Toulouse cedex 4, France
[8] Istituto Nazionale di Astrofisica, INAF-IAPS, via del Fosso del Cavaliere, I-00133 Roma, Italy
[9] Cahill Center for Astronomy and Astrophysics, California Institute of Technology, Pasadena, CA 91125, USA
Received 2015 November 20; accepted 2016 April 14; published 2016 June 8

ABSTRACT

We report on observations of the neutron star (NS) residing in the low-mass X-ray binary 1RXS J180408.9-34205 taken 2015 March by *NuSTAR* and *XMM-Newton* while the source was in the hard spectral state. We find multiple reflection features (Fe K_α detected with *NuSTAR*; N VII, O VII, and O VIII detected in the RGS) from different ionization zones. Through joint fits using the self-consistent relativistic reflection model RELXILL, we determine the inner radius to be $\leqslant 11.1\ R_g$. For a 1.4 $M_\odot$ NS with a spin of $a_* = 0$, this is an inner disk radius of $\leqslant 22.2$ km. We find the inclination of the system to be between 18° and 29°. If the disk is truncated at a radius greater than the NS radius, it could be truncated by a boundary layer on the NS surface. It is also possible that the disk is truncated at the magnetospheric radius; conservative estimates would then imply $B \leqslant (0.3\text{–}1.0) \times 10^9$ G at the magnetic poles, though coherent pulsations have not been detected and the source is not identified as a pulsar.

Key words: accretion, accretion disks – relativistic processes – stars: neutron – X-rays: binaries

1. INTRODUCTION

Low-mass X-ray binaries (LMXBs) consist of a compact object that accretes matter via Roche lobe overflow from a roughly stellar mass companion. Broad iron line profiles have been seen in these accreting systems that harbor a black hole (e.g., Fabian et al. 1989; Miller 2007; Reis et al. 2008, 2009a) or a neutron star (NS; e.g., Bhattacharyya & Strohmayer 2007; Cackett et al. 2008, 2009, 2010; Papitto et al. 2008; di Salvo et al. 2009; Egron et al. 2013; Miller et al. 2013) as the primary accreting compact object. The asymmetrically, broadened profile of the Fe K_α line gives a direct measure of the position of the inner disk since the effects of gravitational redshift and Doppler redshift/boosting on the emission line become stronger closer to the compact object (Fabian et al. 1989).

The Fe K_α line in NS LMXBs can be used to set an upper limit for the radius of NSs since the disk must truncate at or before the surface (Cackett et al. 2008, 2010; Reis et al. 2009b; Miller et al. 2013; Degenaar et al. 2015a). Constraining the radius of the NS can, in turn, lead to narrowing down the equation of state of the cold, dense matter under extremely dense physical conditions (Lattimer 2011). On the other hand, if the accretion rate is low, it may be possible to constrain the stellar magnetic field based on the radius at which the disk truncates (Cackett et al. 2009; Papitto et al. 2009; Miller et al. 2011; Degenaar et al. 2014).

1RXS J180408.9-34205 (hereafter 1RXS J1804) was classified as an NS LMXB after Type I X-ray bursts were detected during the *INTEGRAL* Galactic Bulge Monitoring in 2012 May (Krimm et al. 2015b). The bursts provided an upper limit of 5.8 kpc as the distance to the binary system. Follow-up observations with *Swift* less than 1 month later showed that the NS had returned to quiescence (Kaur & Heinke 2012).

The source remained quiet until early 2015, when it began to show a steady increase of hard X-rays in the 15–50 keV range as seen with *Swift*/BAT (Krimm et al. 2015b). MAXI/GSC also detected a gradual increase in the 2–20 keV band (Negoro et al. 2015), confirming that 1RXS J180408 had indeed gone into outburst. The hard X-ray brightness increased until plateauing at 100 mcrab on 2015 February 5 with a flux ~160 times the quiescent rate (Krimm et al. 2015a). Type I X-ray bursts were again seen during this observation (Krimm et al. 2015a), reaffirming the source's classification as having an NS as its primary. Krimm et al. (2015a) noted that the X-ray spectrum seen was adequately described by a simple absorbed power-law model.

Radio observations performed with the VLA in 2015 March detected the presence of a jet (Deller et al. 2015). *Swift* X-ray spectra were still described by a single power law placing J180408's location on the radio/X-ray luminosity plane consistent with hard-state NS LMXBs (Deller et al. 2015). However, in early April a drop in the hard X-rays was seen with *Swift*/BAT in conjugation with an increase in softer X-ray emission seen by MAXI/GSC (Degenaar et al. 2015b). This suggests that the source entered a soft spectral state. *Swift* spectra could no longer be described by a simple power law but required the presence of an additional disk component and blackbody component (Degenaar et al. 2015b).

We report on observations taken 2015 March by *NuSTAR* and *XMM-Newton* while the source was still in the hard spectral state. We focus on the importance of constraining the NS's inner radius from its reflection spectrum in this state since it is not obscured by thermal emission in the lower energies.

2. OBSERVATIONS AND DATA REDUCTION

2.1. NuSTAR

NuSTAR (Harrison et al. 2013) observed the target for ≃80 ks between 9:21 UT on 2015 March 5 and 7:36 UT March 6 (Obs ID 80001040002). Light curves and spectra were created using a 120″ circular extraction region centered around the source and another region of the same dimensions away from the source as a background using the NUPRODUCTS tool from NUSTARDAS v1.3.1 with CALDB 20150123. There were a total of five Type 1 X-ray bursts present in the light curves. We will report on the bursts in a separate paper. We created good time intervals (GTIs) to remove 100–170 s after the initial fast rise (depending on the duration of the individual burst) to separate these from the steady emission. These GTIs were applied during the generation of the spectra for both the FPMA and FPMB. Initial modeling of the steady spectra with a constant fixed to 1 for the FPMA and allowed to float for the FPMB was found to be within 0.95–1.05. We proceeded to combine the two source spectra, background spectra, and ancillary response matrices via ADDASCASPEC. We use ADDRMF to create a single redistribution matrix file. The spectra were grouped using GRPPHA to have a minimum of 25 counts per bin (Cash 1979). The net count rate was 39.9 counts s^{-1}.

2.2. XMM-Newton

XMM-Newton observed the target on 2015 March 6 (Obs ID 0741620101) on revolution 2791 for 57 ks. The EPIC-pn camera was operated in "timing" (∼41.1 ks) and "burst" (∼9.5 ks) mode during this time with a medium optical blocking filter. The RGS cameras were also operational for ≃55.8 ks. The data were reduced using SAS ver. 13.5. We are primarily interested in the spectra obtained from RGS due to the high resolution. Moreover, the Epic-pn "timing" mode and "burst" mode spectra suffer from pileup and calibration issues (Walton et al. 2012). The net count rate was 210 and 167 counts s^{-1} for the "timing" and "burst" mode, respectively. Even when eliminating the centralmost columns from the observation, the spectra obtained in the different modes did not agree with *NuSTAR* or even each other. *NuSTAR* does not suffer from photon pileup, so we chose to characterize the spectrum through the Fe K band using only *NuSTAR*. During the observation, there were seven Type 1 X-ray bursts that were filtered from the data by GTIs that removed 125–225 s after the initial fast rise depending on the duration of each burst. We then created spectra through RGSPROC that were grouped using GRPPHA to have a minimum of 25 counts per bin to allow the use of χ^2 statistics. There was an average of 2.6 counts s^{-1} for RGS1 and 3.3 counts s^{-1} for RGS2.

3. SPECTRAL ANALYSIS AND RESULTS

We use XSPEC version 12.8.1 (Arnaud et al. 1996) in this work. All errors are quoted at ⩾90% confidence level. We account for the neutral column hydrogen density along the line of sight via tbnew[10] de/wilms/research/tbabs/index.html. The solar abundance was set to WILM (Wilms et al. 2000), and VERN cross sections (Verner et al. 1996) were used. The RGS and *NuSTAR* were considered in the range 0.45–2.1 keV and 3.5–50.0 keV, respectively. The choice of the lower energy bound of *NuSTAR* data was motivated by two high bins in the low energy of the spectrum.

[10] J. Wilms et al. (2016, in preparation), http://pulsar.sternwarte.unierlangen.

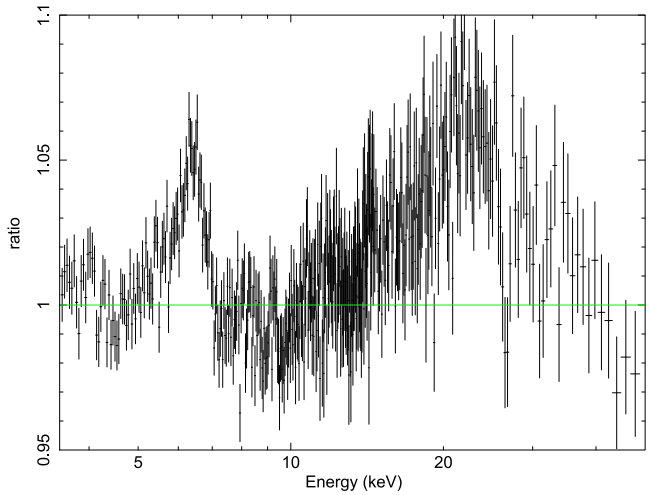

Figure 1. Ratio of the data to the continuum model for *NuSTAR* observations of 1RXS J180408. A simple cutoff power law was fit over the energies of 3.5–5 keV, 8–15 keV, and 30.0–50.0 keV. The iron line region from 5 to 8 keV and reflection hump were ignored to prevent the feature from skewing the fit. We ignore the region above 15 keV in this fit due to the presence of an X-ray reflection hump that peaks between 20 and 30 keV. The data were rebinned for plotting purposes.

3.1. NuSTAR

We start with investigating the *NuSTAR* data alone. Initial fits were performed with an absorbed power law with two Gaussian lines at 10.1 and 11.5 keV to account for instrumental response features (Harrison et al. 2013). These Gaussians will be present in all *NuSTAR* fits hereafter. This gives a particularly poor fit ($\chi^2/\mathrm{dof} = 9545/1159$). The addition of a blackbody to account for the thermal component in the spectrum did not improve the goodness of fit ($\chi^2/\mathrm{dof} = 9545/1157$). The absence of a thermal component is consistent with previous investigations of 1RXS J1804 in the hard state (Deller et al. 2015; Krimm et al. 2015a; Negoro et al. 2015).

A prominent Fe K_α line centered at ∼6.4 keV with a red wing extending to lower energies and Fe edges can be seen rising above the continuum in Figure 1. There is also a prominent reflection hump in the higher energies above 10 keV. These reflection features not being properly described lend to the poor goodness of fit. Since a thermal component is not necessary to describe the spectrum, the only source of emission is a power law. This means that the disk is being illuminated by a source of hard X-ray photons and likely follows a radial dependence R^{-3} profile.

To properly describe the reflection features and relativistic effects present in the data, we employ the model RELXILL (García et al. 2014). This model self-consistently models for X-ray reflection and relativistic ray tracing for a power law irradiating an accretion disk. The parameters of this model are as follows: inner emissivity (q_{in}), outer emissivity (q_{out}), break radius (R_{break}) between the two emissivities, spin parameter (a_*), inclination of the disk (i), inner radius of the disk (R_{in}), outer radius of the disk (R_{out}), redshift (z), photon index of the power law (Γ), log of the ionization parameter ($\log(\xi)$), iron abundance (A_{Fe}), cutoff energy of the power law (E_{cut}), reflection fraction (f_{refl}), angleon, and normalization.

Table 1
Relxill Fitting of *NuSTAR* and RGS

Component	Parameter	*NuSTAR*	RGS	*NuSTAR* + RGS
TBNEW	$N_{\rm H}$ (10^{22})	0.2 ± 0.2	0.360 ± 0.002	0.345 ± 0.001
	A_O	...	1.77 ± 0.01	1.71 ± 0.01
RELXILL	$q_{\rm in} = q_{\rm out}$	$2.4^{+0.5}_{-0.4}$	<1.9	1.3 ± 0.2
	a_*'	0	0	0
	i (°)	25 ± 4	$18.4^{+0.5}_{-0.2}$	18.3 ± 0.2
	$R_{\rm in}$ (ISCO)	$1.9^{+1.4}_{-0.8}$	$1.2^{+3.3}_{-0.2}$	⩽1.85
	$R_{\rm out}$ $(R_g)'$	400	400	400
	z'	0	0	0
	Γ	<1.424	<1.402	1.402 ± 0.001
	log(ξ)	$2.4^{+0.4}_{-0.1}$	3.14 ± 0.03	2.75 ± 0.01
	$A_{\rm Fe}$	$0.83^{+0.4}_{-0.3}$	<0.51	<0.51
	$E_{\rm cut}$ (keV)	45^{+2}_{-1}	30 ± 3	47.3 ± 0.3
	$f_{\rm refl}$	0.15 ± 0.02	0.21 ± 0.01	0.15 ± 0.01
	angleon′	1	1	1
	norm (10^{-2})	$9.5^{+0.3}_{-0.6}$	9.81 ± 0.04	9.35 ± 0.01
RELLINE	$E_{\rm line}$	...	0.569 ± 0.001	0.569 ± 0.001
	norm (10^{-3})	...	6.7 ± 0.8	3.9 ± 0.6
	χ^2_ν(dof)	1.05 (1151)	1.48 (2804)	1.34 (3963)

′ = fixed

Note. Errors are quoted at ⩾90% confidence level. Setting angleon =1 takes the inclination into account when modeling reflection. A constant was allowed to float between *NuSTAR* and the RGS data. The *NuSTAR* was frozen at the value of 1.0, RGS1 was fit at 1.234 ± 0.006, and RGS2 was fit at 1.182 ± 0.005. The emissivity index, inclination, and inner radius in RELLINE were tied to the values in RELXILL. The unabsorbed flux from the combined *NuSTAR*+RGS fit from 0.45 to 50.0 keV is $F_{\rm unabs,(0.45-50.0\ keV)} = 1.71 \times 10^{-9}$ erg cm^{-2} s^{-1}. This gives a luminosity of $L_{(0.45-50.0\ keV)} = 6.8 \times 10^{36}$ erg s^{-1} (~3%–4% $L_{\rm Edd}$).

A few reasonable conditions were enforced when making fits with RELXILL. First, we tie the outer emissivity index, $q_{\rm out}$, to the inner emissivity index, $q_{\rm in}$, to create a constant emissivity index that is allowed to vary between 1 and 3. Next, we fix the spin parameter, a_* (where $a_* = cJ/GM^2$), in the model RELXILL to 0 in the subsequent fits since NSs in LMXBs have $a_* \leqslant 0.3$ (Galloway et al. 2008; Miller et al. 2011). This does not hinder our estimate of the inner radius since the position of the innermost stable circular orbit (ISCO) is relatively constant for low spin parameters. In fact, Miller et al. (1998) found that corrections for frame-dragging for $a_* < 0.3$ give errors $\ll$10%. Further, the outer disk radius has been fixed to $400R_g$ (where $R_g = GM/c^2$). Lastly, to ensure that the inclination is properly taken into account in the reflection from the disk, we set angleon = 1 rather than 0 (angle averaged).

Fits with TBNEW*RELXILL and two Gaussian components, again accounting for instrument response features, provide a significantly better fit (χ^2/dof = 1213/1151). This is well over a 20σ improvement. Values for model parameters are given in Table 1. Figure 2 shows the modeled spectrum and the ratio of the model to the data. The absorption column density is $(2.0 \pm 2.0) \times 10^{21}$ cm^{-2}. The large uncertainties are due to the lack of data in the low-energy range, where X-ray absorption is

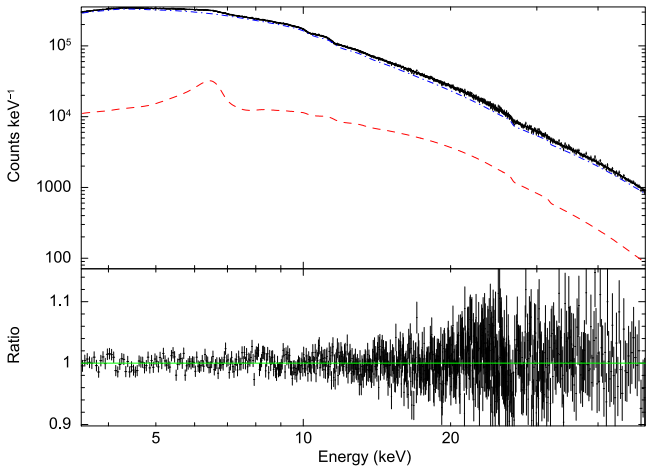

Figure 2. *NuSTAR* spectrum fit with TBNEW*(RELXILL+GAUSS+GAUSS) ($\chi^2_{\rm red} = 1.05$). Gaussians were fit at 10.1 and 11.5 keV to account for instrumental response features. The red dashed line shows the reflection spectrum from the RELXILL model. The blue dot-dashed line shows the power-law component within the RELXILL model. The lower panel shows the ratio of the data to model. The spectrum has been rebinned for plotting purposes. Parameter values can be seen in the third column of Table 1.

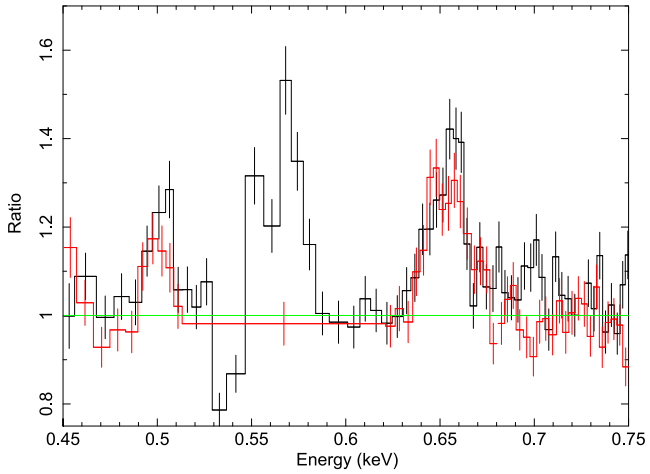

Figure 3. Ratio of the data to the continuum model for *XMM-Newton* RGS1 (black) and RGS2 (red) showing three emission lines (N VII, O VII, O VIII) and O VIII K edge. The continuum was modeled with a simple absorbed power law that was fit over the energies of 0.45–2.1 keV. The N VII line is located near the edge of the effective area of the detector and therefore not modeled in subsequent fits. The data were rebinned and the *x*-axis was rescaled for plotting purposes.

prevalent. The photon index is consistent with the hard limit of 1.4 at the 90% confidence level. The power-law cutoff energy is 45^{+2}_{-1} keV. The inclination of the disk is 25° ± 4°. The parameter of most interest is the inner radius, $R_{\rm in}$, which was found to be $1.9^{+1.4}_{-0.8}$ ISCO.

3.2. RGS

The RGS spectra showed prominent broad features rising above the continuum emission (modeled with an absorbed power law) at ~0.50, ~0.57, and ~0.65 keV corresponding to H-like N VII, He-like O VII, and H-like O VIII, respectively (see Figure 3). Applying simple Gaussian lines places their centroid energy at 0.501 ± 0.002 keV, 0.568 ± 0.002 keV, and 0.655 ± 0.001 keV detected at the 3.2σ, 5.9σ, and 9σ confidence level. To test the robustness of these lines to

Table 2
Emission Line in RGS Spectra

Abs Model	Ion	Lab E (keV)	$E_{\rm centroid}$ (keV)	σ (keV) (10^{-2})	Norm (10^{-4})	Significance (σ)
TBNEW	N VII	0.5003	0.501 ± 0.002	0.6 ± 0.2	1.6 ± 0.5	3.2
	O VII	0.574	0.568 ± 0.002	1.1 ± 0.2	2.9 ± 0.5	5.9
	O VIII	0.654	0.655 ± 0.001	1.2 ± 0.2	4.5 ± 0.5	9
ISMABS	N VII	0.5003	0.501 ± 0.002	0.6 ± 0.3	1.3 ± 0.5	2.6
	O VII	0.574	0.571 ± 0.001	0.8 ± 0.2	2.2 ± 0.5	4.4
	O VIII	0.654	0.654 ± 0.001	1.0 ± 0.2	3.4 ± 0.6	5.7

Note. In TBNEW, all abundances were set to solar with $N_{\rm H} = 2.0 \times 10^{21}$ cm^{-2} (Dickey & Lockman 1990). Normalization is given in units of photons cm^{-2} s^{-1}. An absorbed power law was used to model the continuum. In ISMABS, elemental abundances were allowed to vary. The continuum was modeled with a power law of photon index 1.4.

different assumptions about the interstellar medium, we applied ISMABS (Gatuzz et al. 2014) with the same power-law continuum. The abundance of each element is left as a free parameter so that the photoelectric absorption edges in ISMABS have the greatest possible opportunity to model the data in a way that would remove line-like features. The lines are still present in the spectra, though their significance has decreased slightly, with the N VII line only being marginally significant. We believe the N VII to be a real feature, but due to its location at the edge of the effective area of the detector, we are unable to model it properly in subsequent fits. See Table 2 for the values obtained for the Gaussian lines with each absorption model.

We then applied the self-consistent reflection model RELXILL in combination with TBNEW to describe the lines simultaneously. We allowed the abundance of O to be a free parameter in TBNEW to fully account for the O VIII K EDGE at 0.53 keV, which can be seen in Figure 3. The model was not able to account for the He-like O VII line with the other two H-like lines, likely due to the lower ionization parameter needed to create the line. We employ the relativistic line model RELLINE to describe this feature. The emissivity index, inclination, and inner radius were tied to the parameters in RELXILL. The limb parameter was set to 2 for consistency with RELXILL, which assumes limb brightening. We only allowed the normalization and line energy to be free. The addition of the RELLINE component to RELXILL improves the overall fit by $\Delta\chi^2 = 147$ (for 2 dof). The resulting best fit can be seen in Table 1. The probability of the additional component improving the fit by chance was found to be negligibly small (3.19×10^{-24}) via an F-test. This is a 9.6σ improvement. The unfolded model can be seen in Figure 4. Figure 5 shows the RELXILL-only model decomposed into the continuum and reflection components that are comprised in the model.

The cut energy and emissivity are not well constrained, likely due to limited bandwidth. Again, the photon index is consistent with the hard limit of 1.4 at the 90% confidence level. The absorption column is better constrained than in the previous fit with $N_{\rm H} = 3.60(\pm)0.02 \times 10^{21}$ cm^{-2} with an oxygen abundance 1.77 ± 0.01 solar. The reflection fraction is higher than that of the *NuSTAR* spectrum, meaning that it is dominated by more reflection. The high reflection fraction reaffirms that the emission lines are reflection features. The inclination is several degrees lower than the inclination found in the higher energy range, but is generally consistent. The location of the inner disk ($1.2^{+3.3}_{-0.2}$ ISCO) is compatible with the iron line region.

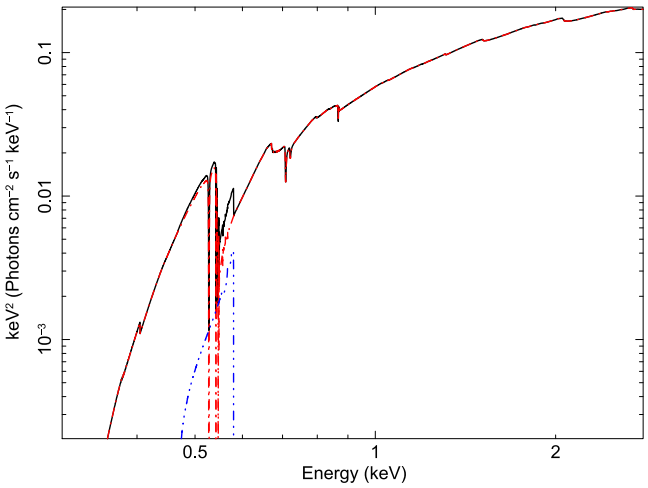

Figure 4. Unfolded model spectrum for *XMM-Newton* RGS. The blue component corresponds to RELLINE. The red component illustrates RELXILL, which includes the power law.

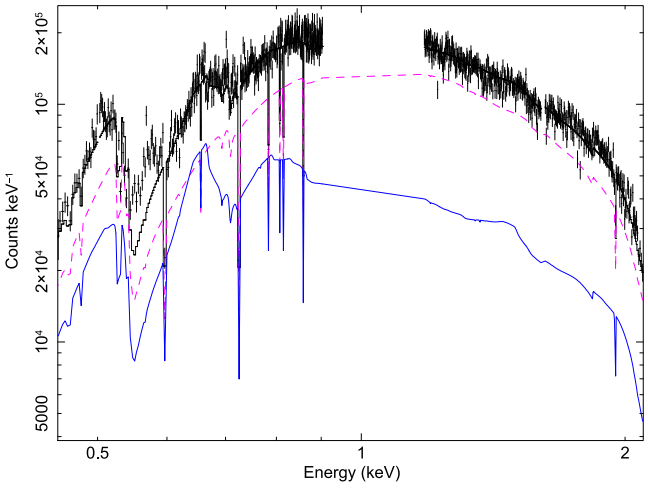

Figure 5. Decomposed RELXILL model spectrum for *XMM-Newton* RGS1 showing the reflection component (solid blue) and power-law continuum (dashed purple). The RELLINE component is not shown to illustrate the model's ability to fit the O VIII line.

3.3. NuSTAR+RGS

Due to the limited energy bandwidth of the RGS, we fit the *NuSTAR* and RGS together in order to obtain better estimates of the spectral parameters of interest. Tying the RGS data with the *NuSTAR* data provides an opportunity to fit multiple relativistic reflection features over a wide energy range

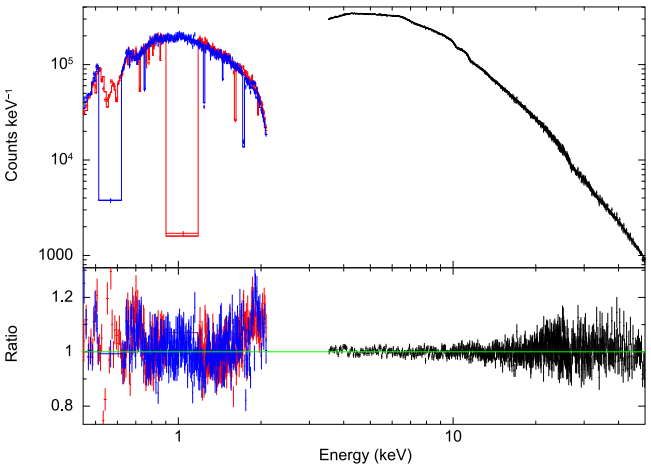

Figure 6. Joint fit of RGS and *NuSTAR* with TBNEW*(RELXILL+GAUSS+GAUSS +RELLINE) ($\chi^2_{red} = 1.34$). The additional RELLINE parameter is needed to model the He-like O VII line. Gaussians were fit at 10.1 and 11.5 keV to account for instrumental response features. The spectrum has been rebinned for plotting purposes. Parameter values can be seen in the fifth column of Table 1.

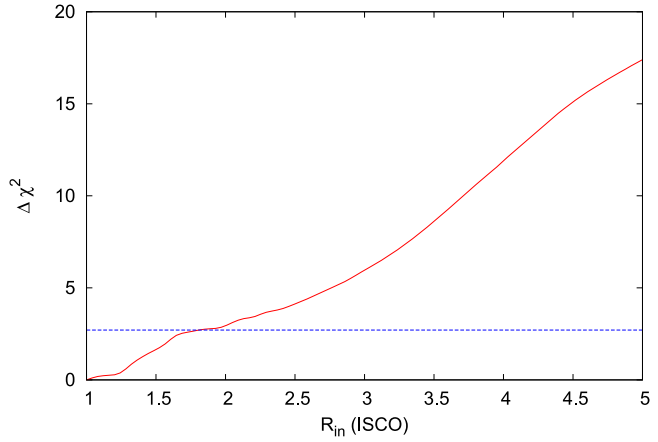

Figure 7. Change in goodness of fit vs. inner disk radius for the *NuSTAR*+RGS column in Table 1 taken over 50 evenly spaced steps generated with XSPEC "steppar." The inner disk radius was held constant at each step, while the other parameters were free to adjust. The blue dashed line shows the 90% confidence level.

(∼0.45–50.0 keV) and from different ionized regions in the disk. A constant was allowed to float between the two observations, but all other model parameters were tied. The constant was frozen at the value of 1.0 for *NuSTAR* and free to vary for RGS1 and RGS2. The constant for RGS1 was found to be $c = 1.234 \pm 0.006$ and $c = 1.182 \pm 0.005$ for RGS2. The model we first use is TBNEW*(RELXILL+RELLINE+GAUSS+GAUSS) to model the relativistic reflection features with X-ray absorption along the line of sight. The Gaussian lines are to account for instrumental response features. See Table 1 and Figure 6.

Simultaneous fits return a neutral absorption column density $N_H = (3.45 \pm 0.01) \times 10^{21}\,cm^{-2}$ with a slight overabundance in oxygen, $O = 1.71 \pm 0.01$ solar. The emissivity index, $q = 1.3 \pm 0.2$, suggests that a large area of the disk is being illuminated by a hard X-ray source. The ionization parameter being $\log(\xi) = 2.75 \pm 0.01$ is within reason for an accreting source in the low/hard state (LHS; Cackett et al. 2010), although there are a number of cases where lower ionizations are found for an NS in the LHS (SAX J1808.4-3658: Papitto et al. 2009; Cackett et al. 2009; 4U 1705-44: D'Aì et al. 2010; Di Salvo et al. 2015). The iron abundance was allowed to be a free parameter and is consistent with the hard limit of 0.5 at the 90% confidence level. The photon index of the power-law component that is responsible for producing the reflection spectrum is on the harder side with $\Gamma = 1.402 \pm 0.001$. The reflection fraction, f_{refl}, is 0.15 ± 0.01. The inclination agrees with the previous individual fit to the RGS data alone. The inner radius, $R_{in} \leqslant 1.85$ ISCO, is consistent within uncertainties with the individual fits to *NuSTAR* and RGS alone. Figure 7 shows the change in χ^2 when stepping the inner disk radius parameter out to 5 ISCO using the "steppar" command in XSPEC.

To explore the multiple ionization parameters that seem prevalent in the RGS data, we remove the RELLINE component and apply a double RELXILL model to the joint spectra. The idea is to be able to map the X-ray interactions with accretion disk radii. We tie the emissivity index, inclination, inner radius, photon index, and iron abundance between the two RELXILL components and allow the ionization, reflection fraction, and normalization to change between them. Parameter values can be seen in Table 3.

Table 3
Double Relxill Fitting of *NuSTAR* and RGS

Component	Parameter	Values
TBNEW	$N_H\,(10^{22})$	0.340 ± 0.003
	A_O	1.689 ± 0.03
RELXILL	$q_{in} = q_{out}$	<1.2
	a'_*	0
	$i\,(°)$	$18.11^{+0.3}_{-0.2}$
	R_{in} (ISCO)	$1.13^{+2.98}_{-0.13}$
	$R_{out}\,(R_g)'$	400
	z'	0
	Γ	<1.41
	$\log(\xi)_1$	2.9 ± 0.1
	$\log(\xi)_2$	1.5 ± 0.2
	A_{Fe}	<0.54
	E_{cut} (keV)	45.1 ± 0
	$f_{refl,1}$	0.2 ± 0.1
	$f_{refl,2}$	0.22 ± 0.02
	angleon$'$	1
	$norm_1\,(10^{-2})$	$4.73^{+2.2}_{-1.3}$
	$norm_2\,(10^{-2})$	$4.68^{+4.7}_{-1.0}$
	χ^2_ν(dof)	1.36 (3962)

$'$ = fixed

Note. Errors are quoted at ⩾90% confidence level. Setting angleon = 1 takes the inclination into account when modeling reflection. A constant was allowed to float between *NuSTAR* and the RGS data. The *NuSTAR* was frozen at the value of 1.0, RGS1 was fit at 1.25 ± 0.01, and RGS2 was fit at 1.19 ± 0.01.

The higher ionization parameter agrees with the values obtained in the previous fits. The lower ionization value accounts for the production of the O VII line. The inner radius, $R_{in} < 4.1$ ISCO, agrees with the value obtained in the previous model when using RELLINE to describe the O VII line, which does not make assumptions about the underlying gas physics like RELXILL does. The reflection fractions for each component are consistent with one another, though the normalization is not

well constrained. We do not expect these two different ionization states to occur at the same radii, and as such, we tried to free the inner radius in each of the RELXILL components to map the radius at which the X-ray interactions with the disk occurred. We were unable to obtain radii that were statistically distinct. The goodness of fit of the double RELXILL model is comparable to the simpler fit with just one RELXILL component and RELLINE. We chose to use the parameter values from the simpler model fits in subsequent calculations.

If the inner disk is truncated substantially above the NS surface itself, as allowed by our upper limits on $R_{\rm in}$, then the disk may instead be truncated by a boundary layer extending from the stellar surface. The upper limit on $R_{\rm in}$ would require a boundary layer that is a few times the stellar radius in size. Alternatively, the disk could be truncated by magnetic pressure. We can place an upper limit on the strength of the field using the upper limit of $R_{\rm in} = 1.85$ ISCO. Assuming a mass of 1.4 $M_{\odot}$, taking the distance to be 5.8 kpc (Krimm et al. 2015b), and using the unabsorbed flux from 0.45 to 50.0 keV of 1.71×10^{-9} erg cm^{-2} s^{-1} as the bolometric flux, we can determine the magnetic dipole moment, μ, from Equation (1) taken from Cackett et al. (2009):

$$\mu = 3.5 \times 10^{23}\, k_A^{-7/4}\, x^{7/4} \left(\frac{M}{1.4 M_{\odot}}\right)^2 \times \left(\frac{f_{\rm ang}}{\eta} \frac{F_{\rm bol}}{10^{-9}\ {\rm erg\ cm^{-2}\ s^{-1}}}\right)^{1/2} \frac{D}{3.5\ {\rm kpc}}\ {\rm G\ cm^3}. \quad (1)$$

If we make the same assumptions about geometry and accretion efficiency (i.e., $k_A = 1, f_{\rm ang} = 1$, and $\eta = 0.1$), then $\mu \simeq 1.62 \times 10^{26}$ G cm^3. This corresponds to a magnetic field strength of $B \simeq 3.2 \times 10^8$ G at the magnetic poles for an NS of 10 km. Moreover, if we assume a different conversion factor $k_A = 0.5$ (Long et al. 2005), then the magnetic field strength at the poles would be $B \simeq 1.0 \times 10^9$ G. We note, however, that coherent pulsations have not been detected in 1RXS J1804, and the source is not identified as a pulsar.

However, if the disk does extend closer to the ISCO, then we can place a lower limit on the gravitational redshift from the NS surface, $z_{\rm NS}$. Gravitational redshift is given by $z + 1 = 1/\sqrt{1 - 2GM/R_{\rm in}c^2}$. For $R_{\rm in} = 1.1$ ISCO, assuming a 1.4 $M_{\odot}$ NS and $a_* = 0$, $z_{\rm NS} \geqslant 0.2$ given that the NS is smaller than the radius of the disk. Our measurement for $R_{\rm in}$ does extend down to 1 ISCO. If this were the case, then $z_{\rm NS} \geqslant 0.22$ for a 12 km NS.

To be thorough, we fix the spin to 0.12 and 0.24 to test our assumption that the position of the inner disk radius changes slowly for low spin parameters as per Miller et al. (2013). The inner radius changes only marginally for the highest spin of $a_* = 0.24$, confirming that our fits are not highly dependent on the choice of spin parameter.

4. DISCUSSION

We have analyzed observations taken of the NS LMXB 1RXS J180408.9-34205 in the hard spectral state. We find clear evidence of a prominent iron line at 6.4 keV in the *NuSTAR* spectra and three reflection lines in the *XMM-Newton*/RGS corresponding to N VII, O VII, and O VIII. This is the first time that a broad iron line has been detected in conjunction with multiple lower-energy lines in the RGS.

We have found that when tying the *NuSTAR* and RGS data together, 1RXS J1804 has an $R_{\rm in} \leqslant 1.85$ ISCO with an inclination between 18° and 29°. This translates to $\leqslant$22.2 km for a 1.4 $M_{\odot}$ NS with $a_* = 0$. Further, we are close to being able to map how ionization varies with radius in the disk. Individual fits to *NuSTAR* and RGS suggest that the O region may be located farther out in the disk than the Fe line region, but uncertainties do not exclude their mutual location.

There are a growing number of NS LMXBs with small inner radius measurements, such as Serpens X-1 (Miller et al. 2013; Chiang et al. 2015) and 4U 1608-52 (Degenaar et al. 2015a). These objects were in a higher spectral state with softer photon indices that required the addition of thermal components in contrast to 1RXS J1804. Both objects had relativistic iron lines emerging from $R_{\rm in} = 6.2$–$7.2\ R_g$ (Miller et al. 2013) for Serpens X-1 and $R_{\rm in} = 7$–$10\ R_g$ (Degenaar et al. 2015a) for 4U 1608-52. Additionally, Cackett et al. (2010) looked at seven other NS LMXBs in addition to Serpens X-1. Nearly all of the objects were found to have an inner radius in the range of 6–15 R_g. The relatively small inner radius measurement obtained for 1RXS J1804 suggests that the disk does not necessarily become highly truncated in the hard state. Similar behavior for the location of the inner radius was also seen for 4U 1705-44 (Di Salvo et al. 2015). The disk radius in the hard state was comparable with the soft state.

The ionization parameter for 1RXS J1804 is comparable to the values seen for other NS reflection studies for the iron line region, $2.3 < \log(\xi) < 4.0$ (Cackett et al. 2010; Miller et al. 2013; Degenaar et al. 2015a). However, other studies find lower ionization parameter values for an NS in the LHS (Cackett et al. 2009; Papitto et al. 2009; D'Aì et al. 2010; Di Salvo et al. 2015). However, it is likely that some of the emergent flux in the iron line region for 1RXS J1804 is partially from a region of lower ionization. Again, we are close to tracing out the ionization as a function of disk radius and will push toward this goal in future work by achieving better overall data quality (higher signal-to-noise ratio). We will focus on obtaining deeper observation with RGS for objects like 1RXS J1804 in the hard state with little to no thermal component to drown out the low-energy reflection features.

If the disk is not truncated at the stellar surface, it may be truncated at the magnetospheric radius. Using conservative methods, we find that the upper limit on $R_{\rm in}$ implied by our fits would limit the magnetic field at the poles to $B \leqslant (0.3$–$1.0) \times 10^9$ G (magnetic field strength at the poles is twice as large as at the magnetic equator). However, pulsations are not seen in this source, and thus our estimate should be considered an upper limit. An alternative explanation for disk truncation may be the presence of a boundary layer between the NS and inner disk (see D'Aì et al. 2010 for more details).

We thank the referee for the generous and helpful comments. We also thank Javier Garcia for insightful discussion regarding the RELXILL model. E.M.C. gratefully acknowledges support from the National Science Foundation through CAREER award number AST-1351222. This research makes use of data from the *NuSTAR* mission, a project led by the California Institute of Technology, managed by the Jet Propulsion Laboratory, and funded by the National Aeronautics and Space Administration. We thank the *NuSTAR* Operations, Software, and Calibration teams for support with the execution and

analysis of these observations. This research has made use of the *NuSTAR* Data Analysis Software (NuSTARDAS) jointly developed by the ASI Science Data Center (ASDC, Italy) and the California Institute of Technology (USA). This research also made use of data obtained with *XMM-Newton*, and the ESA science mission with instruments and contributions directly funded by ESA Member States and NASA. L.N. wishes to acknowledge the Italian Space Agency (ASI) for financial support by ASI/INAF grant I/037/12/0-011/13.

REFERENCES

Arnaud, K. A. 1996, in ASP Conf. Ser. 101, Astronomical Data Analysis Software and Systems V, ed. G. H. Jacoby, & J. Barnes (San Francisco, CA: ASP), 17
Bhattacharyya, S., & Strohmayer, T. E. 2007, ApJL, 664, L103
Cackett, E. M., Altamirano, D., Patruno, A., et al. 2009, ApJL, 694, L21
Cackett, E. M., Miller, J. M., Bhattacharyya, S., et al. 2008, ApJ, 674, 415
Cackett, E. M., Miller, J. M., Bhattacharyya, S., et al. 2010, ApJ, 720, 205
Cash, W. 1979, ApJ, 228, 939
Chiang, C.-Y., Cackett, E. M., Miller, J. M., et al. 2015, ApJ, submitted (arXiv:1604.08626)
D'Aì, A., Di Salvo, T., Ballantyne, D., et al. 2010, A&A, 516, A36
Degenaar, N., Altamirano, D., Dellar, A., et al. 2015b, ATel, 7352, 1
Degenaar, N., Miller, J. M., Chakrabarty, D., et al. 2015a, MNRAS, 451, L85
Degenaar, N., Miller, J. M., Harrison, F. A., et al. 2014, ApJL, 796, L9
Deller, A., Degenaar, N., Hessels, J., et al. 2015, ATel, 7255, 1
di Salvo, T., D'Ai, A., Iaria, R., et al. 2009, MNRAS, 398, 2022
Di Salvo, T., Iaria, R., Matranga, M., et al. 2015, MNRAS, 449, 2794
Dickey, J. M., & Lockman, F. J. 1990, ARA&A, 28, 215
Egron, E., Di Salvo, T., Motta, S., et al. 2013, A&A, 550, A5
Fabian, A. C., Rees, M. J., Stella, L., & White, N. E. 1989, MNRAS, 238, 729
Galloway, D. K., Muno, M. P., Hartman, J. M., Psaltis, D., & Chakrabarty, D. 2008, ApJS, 179, 360
García, J., Dauser, T., Lohfink, A., et al. 2014, ApJ, 782, 76
Gatuzz, E., Kallman, T., García, J., Gorczyca, T., & Mendoza, C. 2014, The X-ray Universe 2014, ed. J.-U. Ness, 253
Harrison, F. A., Craig, W. W., Christensen, F. E., et al. 2013, ApJ, 770, 103
Kaur, R., & Heinke, C. 2012, ATel, 4085, 1
Krimm, H. A., Barthelmy, S. D., Baumgartner, W., et al. 2015b, ATel, 6997, 1
Krimm, H. A., Kennea, J. A., Siegel, M. H., & Sbarufatti, B. 2015a, ATel, 7039, 1
Lattimer, J. M. 2011, Ap&SS, 336, 67
Long, M., Romanova, M. M., & Lovelace, R. V. E. 2005, ApJ, 634, 1214
Miller, J. M. 2007, ARA&A, 45, 441
Miller, J. M., Maitra, D., Cackett, E. M., Bhattacharyya, S., & Strohmayer, T. E. 2011, ApJL, 731, L7
Miller, J. M., Parker, M. L., Fuerst, F., et al. 2013, ApJL, 779, L2
Miller, M. C., Lamb, F. K., & Psaltis, D. 1998, ApJ, 508, 791
Negoro, H., Sugimoto, J., Mihara, T., et al. 2015, ATel, 7008, 1
Papitto, A., D'Aì, A., di Salvo, T., et al. 2008, ATel, 1846, 1
Papitto, A., Di Salvo, T., D'Aì, A., et al. 2009, A&A, 493, L39
Reis, R. C., Fabian, A. C., Ross, R. R., & Miller, J. M. 2009a, MNRAS, 395, 1257
Reis, R. C., Fabian, A. C., Ross, R. R., et al. 2008, MNRAS, 387, 1489
Reis, R. C., Fabian, A. C., & Young, A. J. 2009b, MNRAS, 399, L1
Verner, D. A., Ferland, G. J., Korista, K. T., & Yakovlev, D. G. 1996, ApJ, 465, 487
Walton, D. J., Reis, R. C., Cackett, E. M., Fabian, A. C., & Miller, J. M. 2012, MNRAS, 422, 2510
Wilms, J., Allen, A., & McCray, R. 2000, ApJ, 542, 914